RESEARCH ARTICLE

NANO · MICRO small
www.small-journal.com

Glass-Like Phonon Dynamics and Thermal Transport in a GeTe Nano-Composite at Low Temperature

*R. Cravero, A. Tlili, J. Paterson, M. Tomelleri, P. Marcello, R. Debord, S. Pailhès, O. Bourgeois, F. Hippert, D. Le Qui, J.-Y. Raty, P. Noe, and V. M. Giordano**

In this work, the experimental evidence of glass-like phonon dynamics and thermal conductivity in a nanocomposite made of GeTe and amorphous carbon is reported, which is of interest for microelectronics, and specifically phase change memories. It is shown that, the total thermal conductivity is reduced by a factor of three at room temperature with respect to pure GeTe, due to the reduction of both electronic and phononic contributions. This latter, similarly to glasses, is small and weakly increasing with temperature between 100 and 300 K, indicating a mostly diffusive thermal transport and reaching a value of 0.86(7) $Wm^{-1}K^{-1}$ at room temperature. A thorough investigation of the nanocomposite's phonon dynamics reveals the appearance of an excess intensity in the low energy vibrational density of states, reminiscent of the Boson peak in glasses. These features can be understood in terms of an enhanced phonon scattering at the interfaces, due to the presence of elastic heterogeneities, at wavelengths in the 2–20 nm range. The findings confirm recent simulation results on crystalline/amorphous nanocomposites and open new perspectives in phonon and thermal engineering through the direct manipulation of elastic heterogeneities.

1. Introduction

Nanostructured materials are at the forefront of current research for many applications, specifically, those where thermal management represents an issue, such as thermoelectric energy conversion or microelectronics. Here, the challenge is to reduce the thermal conductivity without affecting the electronic properties. For this, the aim is to reduce the heat transport assured by the lattice vibrations, whose quasi-particle is the phonon, while perturbing as least as possible the electronic contribution. In one word, it is matter of finding the "phonon glass electron crystal" ideal material,[1] i.e., a material which is as bad a thermal conductor as a glass but still a good electric conductor as a crystal. The introduction of interfaces at the nanoscale (from few to hundreds of nm) represents a most promising strategy as they are expected to efficiently scatter phonons, with a lesser effect on electrons. Still, things are not this clear when it comes to nanocomposites, made of the intertwining at the nanoscale of materials with different properties, where not only interfaces are present, but also nanoscale heterogeneities in elastic and thermal properties. Such combination can lead to very different thermal behaviors, from the enhancement of the thermal conductivity[2–5] to its strong inhibition,[6–13] depending on the constituent materials properties, as well as the nanostructure lengthscale and the temperature.[14] Simulations have shown that this panoply of behaviors is due to the non trivial effects of nanoscale heterogeneities on phonons,[15–18] which can also lead to phonon localization[19] or filtering.[20] Most interestingly, the arising of

R. Cravero, A. Tlili, P. Marcello, R. Debord, S. Pailhès, V. M. Giordano
Institute of Light and Matter
UMR5306 Université Lyon 1-CNRS, Université de Lyon
Villeurbanne cedex F-69622, France
E-mail: valentina.giordano@univ-lyon1.fr

R. Cravero, O. Bourgeois
Institut NEEL, CNRS
Université Grenoble Alpes
25 avenue des Martyrs, Grenoble F-38042, France

The ORCID identification number(s) for the author(s) of this article can be found under https://doi.org/10.1002/smll.202310209

DOI: 10.1002/smll.202310209

J. Paterson, M. Tomelleri, P. Noe
CEA, LETI
Université Grenoble Alpes
Grenoble 38000, France

F. Hippert
CNRS, Grenoble INP, LMGP
Université Grenoble Alpes
Grenoble F-38000, France

D. Le Qui, J.-Y. Raty
FNRS and CESAM
Université de Liége
Sart-Tilman 4000, Belgique

glass-specific features in the vibrational dynamics has been observed in molecular dynamics simulations on nanocomposites made of nanocrystalline inclusions within an amorphous matrix. Specifically, it was reported an early deviation of the low frequency phonon density of states from the Debye behavior, leading to a peak reminiscent of the Boson Peak in glasses, well distinct from the Boson Peak of the amorphous matrix.[16] Similarly to this latter, this deviation appears together with a change of the nature of the phonon from propagative to diffusive. As such, simulations point to these nanocomposites as a possible realization of the phonon glass electron crystal. Moreover, while the nature of the Boson Peak in glasses is still matter of debate, one of the proposed interpretations ascribes it to a strong phonon scattering due to the presence of nanometric elastic heterogeneities intrinsic to the disordered state.[21–23] This would suggest a parallel between glasses and nanocomposites, due to the presence in both of elastic heterogeneities, intrinsic to the disorder state in the former and artificially induced in the latter. Such concept, if confirmed, could open new exciting perspectives in phonon thermal engineering. Unfortunately, until now, an experimental confirmation is still missing.

Here, we produce the first experimental evidence of the arising of glass-like dynamics and thermal transport due to nanoscale elastic heterogeneities in a nanocomposite based on germanium telluride (GeTe), of interest for microelectronic, photonic, and thermoelectric applications.

GeTe belongs to the family of chalcogenide materials at the forefront of current research for phase change resistive memories (PCM) in microelectronic devices,[24–26] neuromorphic computing,[27] laser thermal lithography,[28] optically photonic devices,[29] as well as for thermoelectric applications.[30–32] This family has been reported to exhibit a novel kind of atomic bonding, dubbed metavalent, considered to be responsible for a series of properties that make it especially interesting for PCMs and thermoelectrics.[33] In both these applications, the major challenge for reducing energy consumption in the former and improving the figure of merit in the latter, is the reduction of the thermal conductivity. The main strategy has been to increase phonon scattering by doping or alloying[32,34]. In some cases the deposited amorphous alloy has led, upon crystallization, to a phase segregation and the realization of nanodomains of the undoped phase change material separated by another phase. It's the case of $Ge_2Sb_2Te_5$-SiO_x nanocomposites, for which a twofold thermal conductivity reduction was reported for a 5% SiO_x molar content.[35] Very recently, the crystallization of carbon doped GeTe has also been shown to give rise to a nanocomposite made of nanograins of crystalline GeTe (below 20 nm size) interconnected by amorphous carbon, which has proved to efficiently reduce the programming currents in PCM devices, suggesting an important thermal conductivity reduction.[36–38] This, together with an increased thermal stability, due to a higher crystallization temperature in the nanocomposite, points to this material as very promising for PCM applications. Still, to optimize its composition and nanostructure, a microscopic understanding of the effect of this latter on thermal transport is necessary.

Disentangling the many elements which play a role in determining heat transport in GeTe is however not trivial. In bulk GeTe thermal transport is dominated by anharmonic phonon–phonon scattering and scattering from Ge vacancies,[39,40] which are naturally created during crystallization from the amorphous phase, making of GeTe a p-type semiconductor.[41] These mechanisms will be present in the nanocomposite as well, and possibly different. As such, upon nanostructuration, four are the main players: i) Ge vacancy content, ii) anharmonicity, iii) grain size, and iv) the nanoscale heterogeneities due to the contrast of properties between GeTe and amorphous carbon.

In this work, we address these nanocomposites in order to shed light on the microscopic mechanisms behind thermal transport and evidence the effect of the nanostructure. In order to do so, we investigate thermal transport and phonon dynamics at low temperature, where the anharmonic contribution is reduced and nanostructuration effects are expected to be more important. We find that nanostructuration leads to a lattice thermal conductivity between four and seven times smaller than in pure GeTe, for 9% atomic carbon content. Such reduction cannot be explained on the basis of the nanometric grain size or of defect scattering alone, pointing to a major role of boundary scattering whose strength is enhanced by the elastic contrast between the components. Such enhanced scattering leads to the appearance of an excess of modes in the vibrational density of states at wavelengths comparable with the nanostructure lengthscale and to a glass-like lattice thermal conductivity, that we interpret as the result of a dominant diffusive thermal transport.

2. Results

2.1. Samples

Here, we present a thorough investigation of thermal transport and phonon dynamics in a C-doped GeTe thin film with a 9% carbon atomic content (GTC9), compared with the ones in a pure GeTe thin film (GeTe). This carbon amount was chosen as it was enough to induce a strong reduction in the programming currents[42] and thus on thermal transport, without deteriorating too much the electric transport, opposite to higher C content materials, as may be seen in **Table 1**. In order to verify the role of grain size and carbon content we have also prepared a nano-crystalline GeTe (nGeTe) and a nanocomposite with a 16% carbon atomic content (GTC16) for specific measurements. As detailed in the Experimental Section, all samples have been deposited as homogeneous amorphous materials and then

Table 1. Structural, electrical and thermal properties for the samples here investigated. The thermal conductivity was measured by the 3ω technique in all samples, except for nGeTe, for which we used the thermoreflectance technique (see Experimental Section). Values of GTC16 are marked by a star, to mean that these values are affected by a larger uncertainty as only one thickness was available (see Experimental Section).

	GeTe	GTC9	GTC16	nGeTe
grain size (nm)	80(10)	16(3)	13(3)	30(5)
density (g cm^{-3})	6.24(4)	5.86(4)	5.73 (4)	5.76(3)
ρ (μΩ cm)	580(1)	1390(1)	2423(1)	980(1)
n_H (10^{20} cm^{-3})	2.7(1)	11.1(1)	11.5(1)	6(1)
k_T (W/m K)	3.8(1)	1.39(7)	1.0(1)*	3.1(8)
k_{el} (W/m K)	1.310(3)	0.5251(5)	0.32(3)	0.75(5)
k_{ph} (W/m K)	2.5(6)	0.86(7)	0.7(1)*	2.3(8)

crystallized through a controlled annealing up to 500 °C for the nanocomposites and 450 °C for GeTe. In all samples, crystallization of GeTe is accompanied by the expulsion of the excess Ge, which crystallizes at slightly higher temperature (see Experimental Section). Upon crystallization C-doped GeTe expells also carbon, leading to the formation of a nanocomposite made of nanometric crystalline grains of GeTe surrounded by amorphous carbon.[38] nGeTe was prepared by interrupting the annealing just after the crystallization of the expelled Ge, as monitored by reflectivity measurements, and by quenching the sample to avoid any further grain growth. All samples were investigated by x-ray diffraction (reported in Supporting Information), allowing us to confirm the rhombohedral structure of the GeTe phase in all of them. The grain size, as obtained using the Scherrer law, is reported in Table 1, together with the mass density, measured by x-ray reflectivity. The crystalline peaks of expelled Ge are also always present, from which we can estimate an average Ge grain size d_{Ge} = 50.5(9) nm in GeTe and d_{Ge} = 23(7), 15(4) and 18(10) nm in nGeTe, GTC9, and GTC16, respectively.

Concerning the amorphous carbon (a-C) present in the nanocomposites, it is important to estimate its density and fraction of sp^3 bonded carbon atoms, as sound velocity and thermal conductivity strongly depend on these quantities.[43–45] In order to estimate the sp^3 fraction in GTC9, we have measured its Raman spectrum in the frequency region of the amorphous carbon stretching modes. The sp^3 fraction can be estimated from the intensity ratio between the two Raman peaks (see Supporting Information),[44] and the width of the G peak is related to carbon density. We find that our spectrum is compatible with a mostly sp^2 bonded material (60%), and a density of about 2 g cm^{-3}. The carbon volume fraction can be estimated starting from the atomic concentration and the amorphous carbon density. In the literature this latter spans from 1 to 3 g cm^{-3},[43] leading to a volume fraction ψ_{a-C} between 2 and 7% for GTC9 and between 4 and 12% for GTC16. For our estimated carbon density, $\rho = 2$ g cm^{-3}, it is $\psi_{a-C} = 3\%$ for GTC9 and $\psi_{a-C} = 6\%$ for GTC16. Based on the elasticity properties reported for our estimated density[46], the average Debye velocity for amorphous carbon is ≈8.6 ± 1.5 Kms^{-1}. Knowing the Debye velocity for GeTe, $v_{GeTe} \approx 1.9$ Kms^{-1}[47], we can calculate the elastic contrast between the two phases, as the ratio between their acoustic impedences $Z = \rho^M v$, $\chi = \frac{Z_{a-C}}{Z_{GeTe}} \approx$ 1.5(2). We are thus in presence of a good elastic contrast, with the crystalline particles softer than the amorphous network.

2.2. Thermal Conductivity

Figure 1a reports the thermal conductivity of GeTe, GTC9, and amorphous GeTe as a reference for the lowest possible thermal conductivity in pure GeTe. First of all, we remark the very good agreement between our data on GeTe and previous measurements on both amorphous and crystalline GeTe thin films, also reported in the figure.[40,48] The differences can be ascribed to a variable content of Ge vacancies, as a consequence of a different Ge/Te ratio in the as deposited state resulting from sputtering target composition and deposition method. The weaker than 1/T temperature dependence was already reported and ascribed to the combination of Umklapp anharmonic phonon–phonon scattering and vacancy scattering.[39,40]

Concerning GTC9, we observe a strong reduction of the thermal conductivity with respect to GeTe, by a factor of seven at low temperature and four at room temperature and an opposite temperature dependence: rather than decreasing, it slightly increases with temperature. In order to extract the lattice contribution to thermal conductivity, we have measured the electrical conductivity σ and calculated the electronic contribution as: $k_{el} = L\sigma T$, with T the temperature and L the Lorenz number (Wiedemann-Franz law)[49]. As a first approximation, we have extrapolated to our temperature range the Lorenz number calculated in Ghosh et al. for GeTe in the [322–503] K temperature range[40]. Parallely, we have also calculated it using $L = (1.5 + e^{-|S|/116}) \cdot 10^{-8}$ WΩK^{-2}[50] and our measured Seebeck coefficient S, and found that both methods lead to the same lattice thermal conductivity within error bars, with slightly modified absolute values but the same temperature dependence (see Supporting Information).

The electronic contribution, reported in Figure 1b, decreases by a factor between 2.5 and 3.5 going from GeTe to GTC9. This is due to a drastic mobility reduction, as the carrier concentration n_H measured by Hall effect and reported in Table 1 is found to increase by almost a factor of four in GTC9. As holes are provided by Ge vacancies, this increase is due to a larger vacancy content in nanocomposites, likely due to a "Ge-drag" effect during the slow segregation of carbon atoms upon GeTe crystallization. The increased defect scattering from vacancies for holes would thus contribute to reduce the mobility.

Looking now to the pure phononic contribution, reported in Figure 1c, we find that, going from GeTe to GTC9, it decreases by a factor as large as six at low temperature and three at room temperature. Most surprisingly, the GTC9 lattice contribution is found to increase with temperature, with a similar dependence as in amorphous GeTe, suggesting a glass-like thermal transport in this nanocomposite.

2.3. THz Phonon Dynamics

In the Boltzmann transport theory within the single relaxation time approximation, the vibrational contribution from propagative modes to thermal conductivity can be expressed as an integral over all phonon frequencies:[51,52]

$$k_{ph}^{prop} = 1/3 \int C_v(\omega) v^2(\omega) \tau(\omega) g(\omega) d\omega \quad (1)$$

with $C_v(\omega)$ and $g(\omega)$ the phonon specific heat and density of states, v its group velocity and τ its lifetime, measuring the average time between two inelastic scattering processes.

In order to get a better insight on the microscopic mechanisms leading to the strong modification of thermal transport when going from GeTe to GTC9, we have directly looked at individual phonons, by measuring the high frequency vibrational dynamics by Inelastic X-ray Scattering (IXS) at the ID28 beamline of ESRF. Measurements were performed at room temperature on GeTe, GTC9, and also GTC16 to see the effect of a major carbon content. We report in **Figure 2** some representative spectra of the individual phonons for GeTe and GTC9, as collected by IXS at fixed wavevectors q. As our samples are polycrystalline, phonons are measured in the first Brillouin zone and correspond to the orientational average of the branches over all directions.[53]

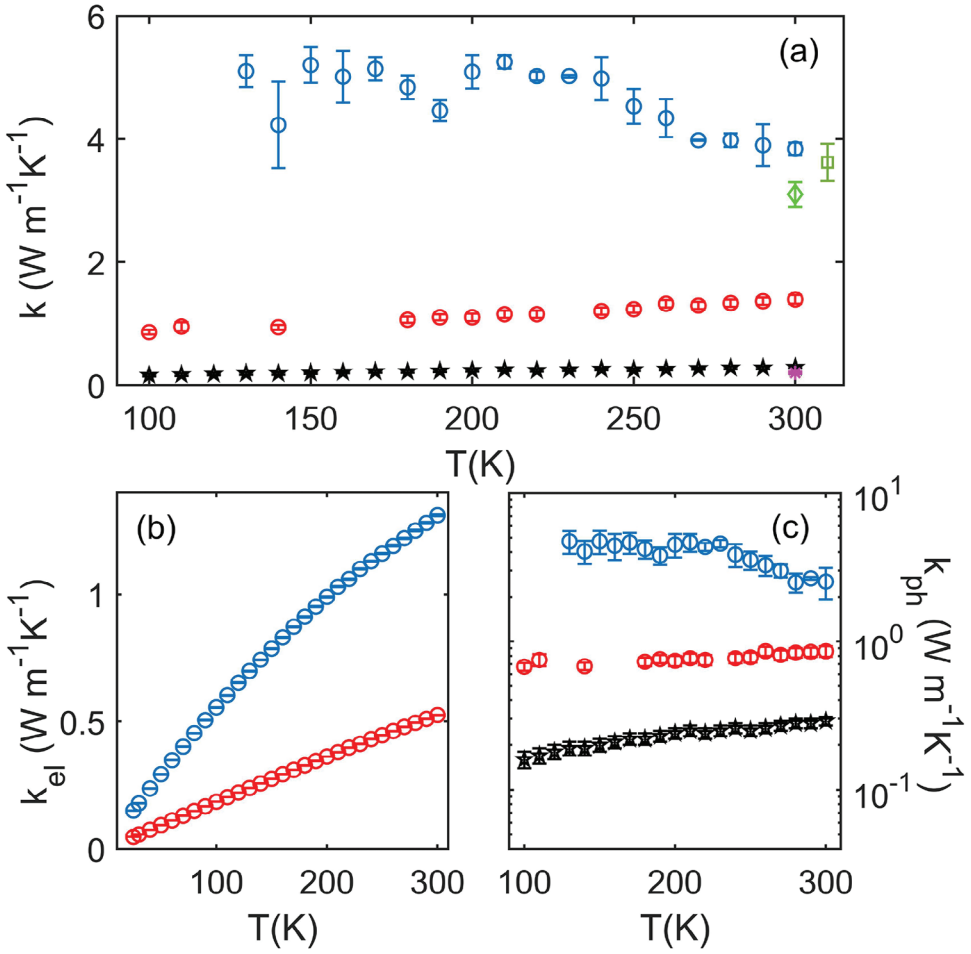

Figure 1. Thermal conductivity. a) The thermal conductivity as measured by the 3ω technique is reported for GeTe (blue circles), GTC9 (red circles squares) and amorphous GeTe (black stars). Literature data for crystalline GeTe (dark green square,[40] light green diamond[48]) and amorphous GeTe (magenta asterisk[48]) are also reported for comparison. Error bars are obtained taking into account the experimental uncertainties on all parameters of the model, using a Monte Carlo procedure, as explained in the Supplementary Material. b) The electronic contribution to thermal conductivity, calculated from the measured electrical conductivity, is reported for GeTe and GTC9. c) The lattice contribution is reported for GeTe, GTC9, and amorphous GeTe in a logarithmic scale to enhance the visibility of the temperature dependences. Error bars are obtained by error propagation on the total thermal conductivity and the electronic contribution.

The intensity of GTC9 data has been rescaled to be exactly on the top of the GeTe ones. In all spectra we can identify a well defined peak, with a high energy shoulder appearing at larger wavevectors: going from GeTe to GTC9 introduces only minor changes and mostly localized on the high energy shoulder. Increasing the C content from 10 to 16% does not introduce any relevant difference (reported in the Supporting Information). We have fitted these data using a model with a variable number of excitations, from 1 to 3 depending on the q value, all represented by a Damped Harmonic Oscillator (DHO) (see Supporting Information). Our results for the phonon dispersions are reported in **Figure 3** together with the theoretical ones calculated ab initio for a pure GeTe at 300 K.

It is worth noticing that our data represent the first experimentally measured phonon dispersions in rhombohedral GeTe. It may be seen that GeTe data are in a very nice agreement with calculations: the low energy mode can be identified as a longitudinal acoustic mode, averaged over the longitudinal branches. The high energy shoulder is made of several modes belonging to different optic branches. In our experimental geometry, we are mostly sensitive to longitudinal density–density fluctuations. Still, in polycrystalline materials, towards the end of the Brillouin zone, it is usually possible to see also transverse modes. It is not our case. The lower energy ones are likely hidden by the intense elastic line, while the higher energy ones could be indistinguishable from the longitudinal ones within their experimental width.[53] Overall, GTC9 and GTC16 well overlap the GeTe data, with no significant differences in the energy position, nor in phonon broadening, as can be seen from Figure 2. It is worth reminding here that in polycrystalline samples the observed phonon linewidth is made of three contributions: the experimental resolution, the width of the phonon distribution over all directions, i.e., the inter-branches separation, and finally the intrinsic phonon broadening, inversely proportional to phonon lifetime.[52,53] In our case, the experimental broadening in the acoustic region is fully determined by the former two

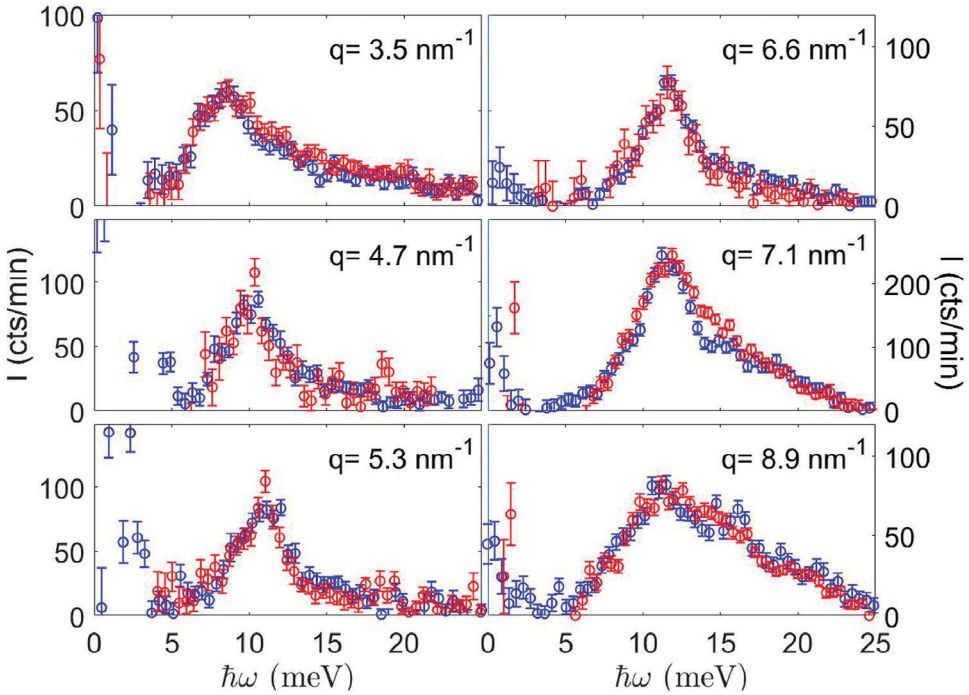

Figure 2. Inelastic x ray scattering spectra. Some representative inelastic x ray scattering spectra collected on GeTe (blue circles) and GTC9 (red circles) are reported at the wavevector values indicated in each panel. GTC9 spectra have been rescaled on the GeTe one to easy the comparison. For better visibility, spectra have been subtracted of the elastic line, and we only show the positive exchanged energy side. Error bars correspond to the Poissonian error on the scattered intensity.

contributions, i.e., we could not extract a phonon intrinsic linewidth. Our experimental conditions set in fact a low limit for the detectable intrinsic width that lies between 0.6 and 1.5 meV depending on q, corresponding thus to an upper limit on the detectable phonon lifetime and mean free path of 1 – 2 ps and ≈5 – 10 nm, respectively.[52] The real intrinsic width and mean free path are therefore respectively below and above such limits, so that we can only conclude that phonon mean free path in both GeTe and GTC9 is longer than 5–10 nm.

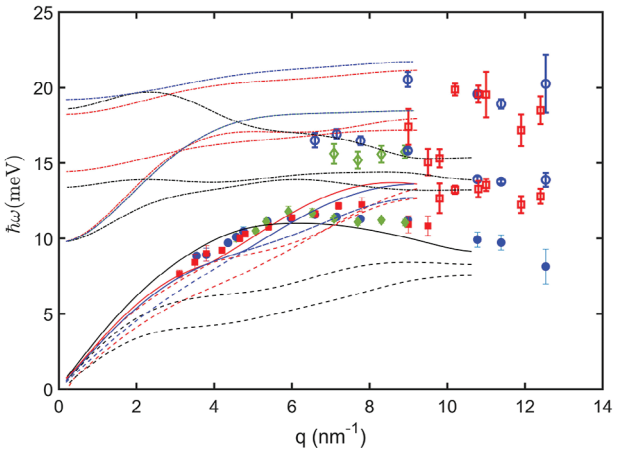

Figure 3. Phonon dispersions. The experimental phonon energy $\hbar\omega$ with respect to wavevector in absolute units q are reported for GeTe (blue bullets), GTC9 (green bullets) and GTC16 (red bullets), together with ab initio calculations for the main symmetry directions in pure GeTe at 300 K (dashed lines: transverse acoustic phonons, solid lines: longitudinal acoustic phonons, dot-dashed lines: optic modes): Γ – L (red), Γ – X (black), Γ – T (blue) (see Experimental Section for their definition). Experimental data correspond to the average of different longitudinal branches over all directions.

Despite the sizable effect on thermal transport, which clearly points to a major change in phonon dynamics, we do not observe it within our experimental resolution. However, such change is expected to mostly concern phonons with wavelengths comparable to the nanostructure lenghscales: the amorphous carbon thickness and the GeTe grain size, i.e., between 1 and ≈16 nm.[38] These wavelengths could not be accessed in our experiment because of the strong small angle scattering, the smallest measured wavevector being q = 3.5 nm^{-1}, corresponding to a maximum phonon wavelength λ = 1.8 nm.

In order to access this scale, corresponding to energies smaller than 7 meV, we have measured the vibrational density of states (DOS) using the Inelastic X-ray Scattering technique with Nuclear resonance Analysis (IXS-NRA) at the ID18 beamline of ESRF.[54] Measurements have been performed at 50 K, for avoiding any spurious effect coming from the multi-phonon contribution subtraction at temperatures higher than the Debye temperature, which is around 180 K for GeTe.[39] Some room temperature scans have also been collected on GeTe and GTC16 for following the modification of the DOS with temperature (shown in the Supporting Information). Previous data in the literature have been reported only on the partial Te density of states at 30 K, using the same technique,[47] and on the neutron-weigthed density of states of a powder GeTe bulk sample at room and higher temperature.[55] A comparison is reported in the Supporting

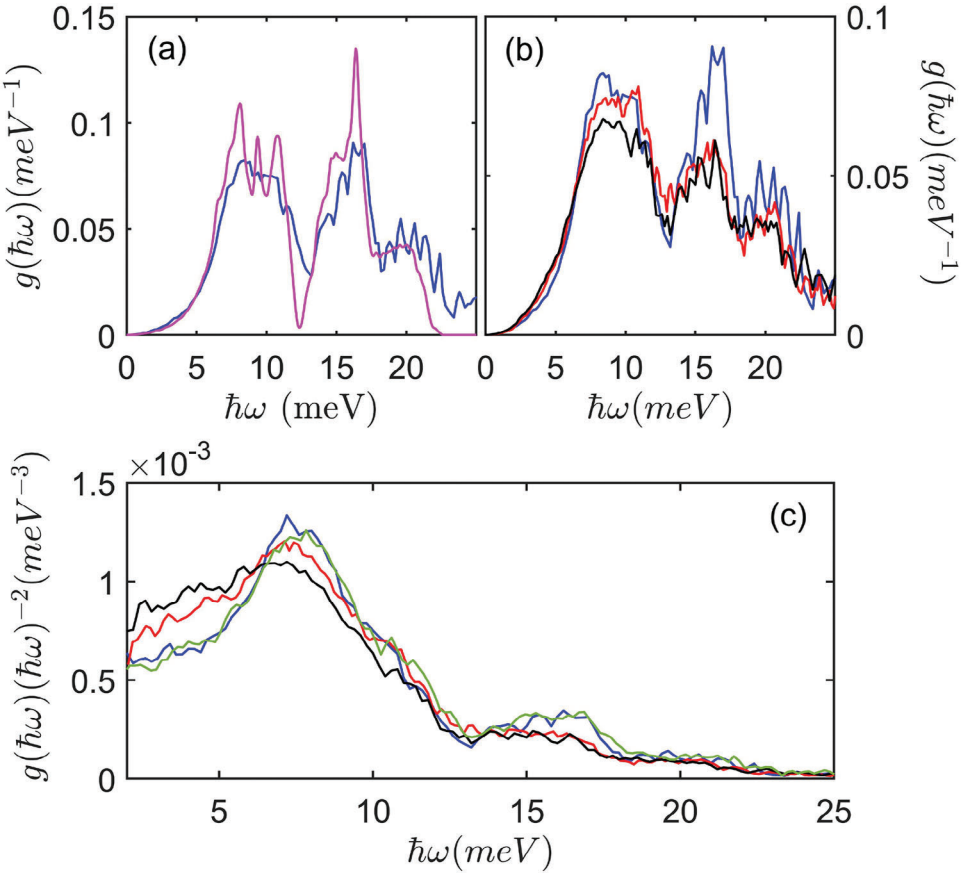

Figure 4. Phonon density of states. a) Phonon density of states as measured using the IXS-NRA technique on GeTe at 50 K (blue) compared with the one calculated ab initio (magenta). b) Phonon density of states at 50 K for GeTe (blue), GTC9 (red), and GTC16 (black). A general broadening is observed in the nanocomposite, as well as modifications in the acoustic region. c) Reduced phonon density of states for GeTe (blue), nGeTe (green), GTC9 (red) and GTC16 (black), showing the growing up of an excess intensity in the 5 meV region in the nanocomposite, increasing with carbon content.

Information, showing a reasonable agreement. In **Figure** 4, we report the DOS as measured in GeTe, compared to the theoretically calculated one (panel (a)) and to GTC9 and GTC16 (panel (b)), all of them measured at 50 K. Once again, we notice the very good agreement with our theoretical results for pure GeTe. Referring to Figure 3, we can easily identify the dip at ≈13 meV as the end of the acoustic regime, the large maximum preceding it corresponding to the different Van Hove singularities coming from longitudinal and transverse branches in the various directions. The two other bands, centered at 16 and 20 meV correspond to bundles of optic modes, that we have measured by IXS.

The DOS is significantly modified in the nanocomposites. It is worth mentioning that, for GeTe, the integrated DOS up to 32 meV is here normalized to 1, as all modes lie in the investigated energy range. This is not true for GTC: additional modes are present at larger energies, due to the amorphous carbon component. Still, the carbon modes give only a negligible contribution below 30 meV, so that the total area of our measured DOS below 32 meV is basically proportional to the GeTe concentration in GTC: 0.91 for GTC9 and 0.84 for GTC16, as we confirmed with theoretical calculations. We have thus accordingly normalized the integrated DOS for the nanocomposites reported in Figure 4. Besides the different area, the evident difference in the DOS of the nanocomposites is an overall broadening, as well as a slight downshift of the optical bands with respect to GeTe. In order to better inspect the acoustic region, we report in panel (c) the DOS normalized to the expected Debye dependence at low energy: $g(\hbar\omega)/(\hbar\omega)^2$. While in GeTe, we observe the expected Debye behavior up to ≈4 − 5 meV, this is not the same in the nanocomposites: low energy intensity starts to raise already at our lowest measured energy point (2 meV for GTC9 and 1.6 meV for GTC16), leading to an excess of intensity over the Debye level at about 4 meV before reaching the acoustic Van Hove singularity. Moreover, this excess intensity, reminiscent of the Boson peak in glasses, increases with carbon content. This perturbed energy range corresponds to the perturbation of acoustic phonons with wavelengths between 2.5 and 10 nm, i.e., within the range expected to be affected by nanostructuration.

3. Discussion

We have seen that the nanocomposites exhibit both glassy phonon dynamics and glassy thermal conductivity behavior. Going from GeTe to GTC, there are several structural modifications which add to phonon scattering: 1) grain size is reduced from 80 to ≈15 nm; 2) the vacancy content increases by a factor of

4; 3) there are heterogeneities of elastic properties at the nanoscale because of the presence of amorphous carbon. In order to disentangle the effect of all these modifications on dynamics and thermal transport, we have first investigated a nanocrystalline GeTe sample (nGeTe), with average grain size 30(5) nm. As can be seen in Table 1, the room temperature thermal conductivity is slightly lower than in GeTe, although it remains within error bars. However, the slight decrease is essentially the result of a reduction in the electronic contribution, while the phononic contribution is indistinguishable within error bars from the one of GeTe. Moreover, the phonon density of states, also reported in Figure 4c, still follows at low energy the Debye behavior. It could be possible that modifications in the DOS could arise only for a smaller grain size, such as in the nanocomposites (≈15 nm). Still, the excess intensity at low energy increases with carbon content, although grain size is almost unchanged between GTC9 and GTC16, suggesting thus that this parameter is not responsible for the observed modifications. The same considerations hold for the role of vacancy scattering or scattering from expelled Ge nanograins, as the vacancy content and Ge grain size remain almost constant with carbon content in the nanocomposites. In order to get an indication on the effect of a larger carbon content on thermal transport, we have also measured the thermal conductivity of GTC16 at room temperature. Unfortunately, this nanocomposite was available in only one thickness, 1μm, thus, in order to get the intrinsic thermal conductivity, we have assumed that the interfacial thermal resistance was the same as in GTC9, based on the similar microstructure. With this assumption, we find a further 30% reduction in the total thermal conductivity, which can mostly be ascribed to the strong reduction of the electronic contribution, with only a minor effect on the lattice contribution, which decreases by 10%. We can thus conclude that the excess of modes in the low energy vibrational density of states and the drastic change in the thermal conductivity are the consequence of the presence of amorphous carbon.

In order to estimate the relative importance of the carbon effect over grain size and vacancy scattering, we fit our thermal conductivity data of GeTe as a function of temperature, using Equation (1) limited to acoustic modes and using wordour experimental results for phonon dispersions and density of states. Phonon lifetime can be calculated using the Mathiessen rule, $\frac{1}{\tau} = \Sigma_i \frac{1}{\tau_i}$, where τ_i is the lifetime associated to the i scattering process. We consider three contributions (anharmonic Umklapp scattering, defect scattering from vacancies and scattering from grain boundaries):

$$\tau_U(\omega, T)^{-1} = B\omega^2 T e^{-\frac{\Theta_D}{3T}} \tag{2}$$

$$\tau_{def}(\omega)^{-1} = \frac{\Gamma_{\text{def}}(\omega)}{2\hbar} \tag{3}$$

$$\tau_{GB}^{gray}(\omega)^{-1} = \frac{1}{P_{GB}} \frac{v_g(\omega)}{d} \tag{4}$$

where B is the strength of Umklapp scattering and $\Theta_D = 180$ K[39] is the Debye temperature in GeTe. In order to model the lifetime contribution due to defect scattering, we need to model the defect induced attenuation Γ_{def}, for which we use a simple analytical model successfully used in mass disorder alloys:[56,57] this gives $\Gamma_{\text{def}} = \pi/2(\hbar\omega)^2 g(\hbar\omega)\langle\epsilon^2\rangle$, where $g(\hbar\omega)$ is the DOS, and ϵ represents the sum of all fluctuations contributions (mass, elastic constants, atomic size).[58] We find that phonon broadening due to Ge vacancies does increase going from GeTe to the nanocomposites, as expected. However, it remains below 0.15 meV, corresponding to lifetimes much longer than 10 ps, which is the reason for which we could not observe it in our IXS experiment. Concerning scattering from grain boundaries, the phonon mean free path will be proportional to the average grain size d (and thus phonon lifetime proportional to d/v_g with v_g the group velocity), weigthed by a factor P_{GB} which takes into account the transmission through the grain boundaries, as well as the quality of the interface. As a first approximation we have used the "gray" model, where the parameter P_{GB} accounts for the effect of grain boundary transmission, though neglecting its energy dependence, which has been found to be relevant mostly at temperatures lower than ours.[59] We note that, in this calculation, we have only used the measured average longitudinal acoustic dispersion, which however is quite representative of an average acoustic dispersion, as theoretical calculations show that many transverse branches have energies similar to the longitudinal ones. As we show in the Supporting Information, using longitudinal and transverse branches calculated by DFT changes only slightly the values of the fitted parameters, without modifying the physical result. For the density of states, we have used the experimental one measured at 50 K. As shown in the Supporting Information, using the one at 300 K does not introduce any significant difference, as the acoustic region is almost unchanged upon temperature.

As can be seen in **Figure 5**, this model gives a good match of the experimental data for GeTe, with $B = 6.6(8)\ \ 10^{-5}$ (meV K)$^{-1}$, and $P_{GB} = 0.30(8)$. A reduced transmission, as indicated by the value of P_{GB}, accounts here for the interface roughness, the crystalline orientation mismatch between neighboring grains and the presence of porosity.

As a first step, we neglect the nanocomposite nature of GTC9, and estimate the effect of a reduced grain size and increased vacancy content on thermal conductivity, using the parameters B and P_{GB} identified for GeTe, and grain size and density of states of GTC9. This estimation is reported in Figure 5b as a black dashed line: it clearly lies well above the experimental one, and keeps a decreasing temperature dependence, confirming that these two scattering sources are not sufficient for inducing the observed thermal transport modification.

As a second step, we consider GTC9 as a GeTe material with "thick and decorated" grain boundaries, including the effect of the amorphous component in an enhanced boundary scattering. For this, we let free both the phonon transmission, which will now be related to the elastic contrast between GeTe and amorphous carbon, and the anharmonic scattering parameter. Indeed, the slight softening of the optic bands in the nanocomposite DOS suggests a possibly higher anharmonicity. As can be seen in the figure, the fit with this model is not able to reproduce the temperature dependence of the experimental data, despite it decreases the Umklapp parameter down to zero. As for the grain boundary scattering, it results $P_{GB} = 0.084(4)$, i.e., a ≈70% reduction

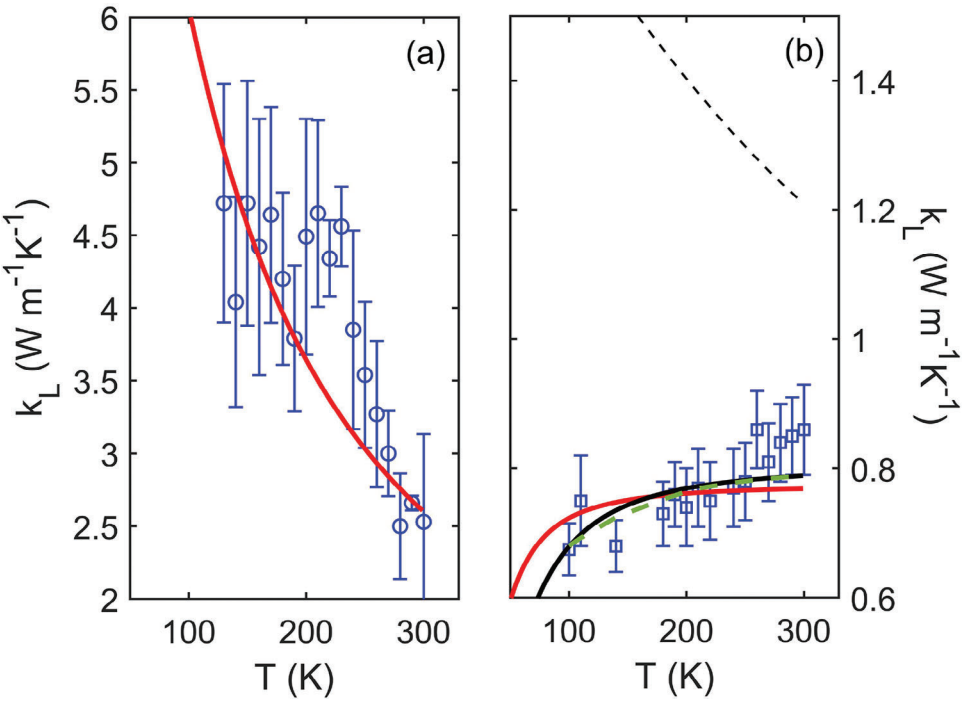

Figure 5. Fit of experimental thermal conductivity. a) The lattice thermal conductivity of GeTe is reported together with the fit Equation (1) and the gray model for boundary scattering (red solid line). b) the lattice thermal conductivity of GTC9 is reported together with the estimated thermal conductivity from GeTe just changing defect scattering and grain size (dashed-dotted black line). The thick red solid line is the fit with Equation 1 and the gray model for boundary scattering, letting the Umklapp parameter go to 0. The thick black solid line is the same fitting with the addition of a diffusive optic contribution. The thick green dashed line represents the fit with an EMA approach, including the Kapitza interfacial resistance.

of the transmission at boundaries: this is the expected stronger boundary scattering due to the elastic contrast at the interfaces. It is worth noticing that the same value for P_{GB} is obtained even if we impose a positive value for B. While this lower transmission may help understanding the absolute value of the thermal conductivity, it cannot explain its temperature dependence. This latter clearly points to a thermal transport dominated by diffusive contributions, that we have not modelled here, where we have only used the propagative acoustic dispersions. Using the theoretical dispersions, we have estimated the diffusive contribution coming from the optical branches and found that it represents less than 10% of the total thermal conductivity in GeTe, but up to 27% in GTC9 at room temperature, as shown in the Supporting Information. We have thus performed the same fit but including the diffusive contribution from optical modes in GTC9 k_{ph}^{diff}, thus fitting our data with $k_{ph} = k_{ph}^{prop} + k_{ph}^{diff}$. In this way, we obtain the black solid line reported in the figure, with P_{GB} = 0.054(3) and B once again equal to zero. The agreement with experimental data is much better, especially at the lowest temperatures and an increasing behavior is now more pronounced. Still, this model neither cannot fully account for the experimentally observed increase. This residual diffusive contribution is likely due to a strong phonon diffusion at the interfaces enhanced by the elastic contrast.

A dominant diffusive thermal transport and a thermal conductivity increasing with temperature was indeed reported in amorphous/crystalline silicon nanocomposites, although for much larger amorphous contents, of 50 and 70%.[16,60,61] The temperature increase was ascribed to the predominance of diffusive vibrational modes and to the Kapitza interface resistance, which decreases with temperature.

We have tried then an effective medium approach (EMA) by fitting our GTC9 data starting from the thermal conductivities of GeTe, modified for the grain size and vacancy content as in Figure 5(b), and the thermal conductivity of an amorphous carbon with similar density and sp^3 content as ours from literature.[43] In order to account for the Kapitza interface resistance, R_K, we have used the formulation by Minnich et al.,[62] with the thermal boundary resistance as only free fitting parameter. As reported in the Supporting Information, the best fit is obtained assuming a linear dependence of the interfacial thermal conductance on temperature, i.e., $R_K = \frac{1}{A+BT}$, with A = 100(10) MW K^{-1}m^{-2} and B = 0.44(6) MW K^{-2}m^{-2}. The order of magnitude for the obtained interfacial thermal conductance is compatible with typical values for a mild contrast of properties.[63] The fit is reported in Figure 5, showing an agreement similar to the one obtained including optic diffusive modes. We notice that, in this EMA approach we could not account for a larger weight of the optic diffusive contribution, which could be at the origin of the remaining discrepancies. It is worth mentioning, that another diffusive contribution could come from a mechanism of mutual coherence, as recently proposed for amorphous materials and complex crystalline systems.[64–67] In these latter, it has been shown that, if optic modes are densely packed, so that

their energy separation is smaller than their broadening, they may coherently interfere, leading to a diffusive transport of energy which tunnels from one mode to the other. Our IXS data do not show any significant change in phonon dispersions with carbon doping, however, the general broadening of the density of states points to a shorter lifetime also for optic modes, which may eventually lead to the realization of the conditions for mutual coherence. More investigations would be needed for testing this hypothesis, specifically calculating the coherent contribution to thermal transport in this material.

Our data could thus be explained on the basis of a mainly diffusive thermal transport mechanism. On one side, the propagative contribution is reduced due to scattering from defects and interfaces, thus giving a major weight to the diffusive contribution from optic modes. On the other side, these latter cannot account for the whole diffusive contribution, which is related to a dominant interface scattering, which can be modeled with the Kapitza resistance. From a microscopic point of view, it likely leads to a change of nature from propagative to diffusive of the GeTe modes with energies corresponding to the excess intensity in the DOS, in agreement with the theoretical predictions.[16] In our case, however, phonons with higher energy are still propagative, as we have seen in our IXS measurements, suggesting an effect of the nanostructure limited to phonons with wavelengths longer than 2 nm (and energies corresponding to the DOS excess intensity), which are mostly diffusively scattered at the interfaces. Molecular dynamics simulations on the real system are planned for identifying the effect of the nanostructuration on such phonons and the origin of the diffusive thermal transport.

4. Conclusion

We have presented an experimental study of thermal transport in a GeTe nanocomposite made of nanograins of crystalline GeTe intertwinned with amorphous carbon, combining the macroscopic measurement of thermal conductivity with the microscopic investigation of phonon dynamics in the meV energy range. We have found that, the total thermal conductivity is reduced by a factor of seven at low temperature and four at room temperature, due to a concomitant reduction of both electronic and lattice contributions. This latter, of only 0.87(7) $Wm^{-1}K^{-1}$ at room temperature, exhibits a glass-like behavior, increasing with temperature. We have shown that, the low value of the lattice thermal conductivity can be explained by an enhanced boundary scattering, whose strength is much larger than in nanocrystalline GeTe, due to the elastic contrast with amorphous carbon. The glass-like temperature dependence can be understood in terms of a dominant role of boundary scattering and diffusive vibrational modes, as already reported in theoretical studies on amorphous/crystalline nanocomposites.[16,60,61] Indeed, not only the diffusive contribution from optic modes becomes more important in GTC9 with respect to GeTe, but also, similarly to the molecular dynamics studies, an excess intensity is found in the density of states at wavelengths comparable with the nanostructure lengthscale, suggesting that acoustic modes with those energies are strongly scattered by the elastic nanoheterogeneities and loose their propagative character contributing thus diffusively to thermal transport. In order to definitely confirm this interpretation, it is necessary to obtain a direct measurement of phonon attenuation at wavelengths between 2 and 20 nm, for which other experimental techniques are needed. This is the case of the laser ultrasonics, which has already been successfully used in GeTe, although at longer wavelengths.[68]

It is worth underlining that the lattice thermal conductivity value obtained at room temperature for GTC9 is comparable with what has been obtained in other GeTe-based materials developed for thermoelectric applications (see Ref. [69] and references therein for a review). Specifically, doping or co-doping to introduce point defect scattering has led to $k_L = 0.6 - 1.4$ $Wm^{-1}K^{-1}$, the lowest value corresponding to $Ge_{0.5}Pb_{0.1}Bi_{0.4}Te$,[70] i.e., an already strongly modified stochiometry. Similar values have also been obtained in solid state solutions and ascribed to phonon scattering by nanoprecipitates. Specifically, the pseudo-binary alloys $(GeTe)_x(AgSbTe_2)_{100-x}$ (TAGS-x), exhibit $k_L = 0.8$ $Wm^{-1}K^{-1}$ for x = 85,[71] and a ultralow $k_L = 0.5$ $Wm^{-1}K^{-1}$ was obtained in $(GeTe)_x(AgSbSe_2)_{100-x}$ (TAGSSe-x) for x = 80,[72] as well as in $Ge_{1-x}Pb_xTe$ with x = 0.13-0.25[73] due to the presence of nanoprecipitates with size ranging from a few to tens of nm. Moreover, there is still room for improvement in GTC nanocomposites. Indeed, as the DOS excess intensity becomes more important and the thermal conductivity gest smaller with increasing carbon content, an even more diffusive behavior could be expected in richer carbon nanocomposites, which could thus allow to achieve the amorphous limit.

On a more general ground, beyond the specific case of GeTe, these results give an experimental evidence of a glass-like phonon dynamics and thermal transport in a nanocomposite, which confirms the many recent theoretical results and allows to assess the parallelism between nanocomposite and glasses, due to the presence in both of elastic heterogeneities. It is important to notice that, the relevance of the evidenced mechanism will depend on the actual material investigated and the temperature range of application, as phonon lifetime is the result of a competition between different scattering mechanisms, which is phonon wavelength and temperature dependent. We expect this enhanced scattering to effectively affect thermal transport in materials where intrinsic phonon mean free paths are longer than the nanostructure lengthscale down to nanometric phonon wavelengths. When this is the case, our findings open the way to the possibility of engineering materials with glassy thermal features by directly manipulating the distribution of the elastic heterogeneities: tuning its strength by choosing the component materials, thus the elastic contrast, and selecting the wavelength range of the affected phonons by choosing the nanostructure lengthscale.

5. Experimental Section

Sample Synthesis and Characterization: Thin films of variable thickness of the homogeneous amorphous alloy $GeTe_{1-x}C_x$ (GTC) had been synthesized by magnetron co-sputtering from a GeTe and a C target in Argon atmosphere on a 200 nm silicon wafer. For electric measurements, a 500 nmm SiO_2 layer was added on top of the wafer. All the films were then capped in situ with 20 nm amorphous SiN for avoiding any oxidation. Two C atomic contents were studied in this work, 9.1 (GTC9) and 16% (GTC16), and obtained by changing the relative sputtering powers applied to the two targets. The Ge and Te concentrations were assessed by Rutherford Back Scattering (RBS), while the one of C by Nuclear Reaction Analysis (NRA). The thickness and density were measured by

X-Ray Reflectivity both at the CEA-LETI and at SOLEIL synchrotron radiation source, at the DiffABS beamline (XRR). The amorphous alloy had been previously investigated both experimentally and theoretically,[42,74] revealing no phase-separation. GTC amorphous phase was a homogeneous alloy where C was present in C chains of various lengths (2–5 atoms), but bonded to Ge and, with a less extent, to Te. A thermal annealing with a ramp rate of 10 Kmin^{-1} was performed for inducing crystallization, while monitoring in situ the electrical resistivity by a four point probe method. The dramatic decrease of the resistivity allowed indeed to clearly identify the crystallization onset and completion, as well as the crystallization of the excess Ge, which was expelled during the process.[38,42] As the crystallization temperature strongly increases with C content,[42] all GTC films were annealed up to 500° C, temperature at which the crystallization process was found to be complete for all C contents. Pure GeTe was prepared following the same procedure, carrying the annealing up to 450° C, for letting the grain grow (GeTe), and in one case stopping it just after crystallization completion, at ≈310 ° C, and quenching the sample, for stopping the grain growth and obtaining a sample with nanometric grains (nGeTe).

Crystalline structure was investigated by X ray diffraction at the diffraction center Henry Loncharbon (Lyon, France), using a Bruker D8 diffractometer in Bragg-Brentano Geometry with $\lambda = 1.54$ Å and a θ-2θ geometry. LaB_6 and Al_2O_3 powder were used to calibrate the diffractometer resolution. Transmission electron microscopy was used to investigate the microstructure of nanocomposites. More details are in the Supporting Information. The Raman signal from amorphous carbon in GTC9 was collected using a LabRAM HR Evolution Raman Spectrometer, from Horiba Scientic, at the Centre Commun de Microspectrometrie Optique (CECOMO) in Lyon, with a laser wavelength of 532 nm, and in a backscattering configuration.

The Hall resistivity, giving access to the charge carrier density, was measured at CEA-LETI SPINTEC varying the magnetic field between −1.5 and +1.5 T, perpendicularly to the surface of the sample. An applied current of 100 µA was imposed between two terminals and the voltage measured between the other two, in a Van Der Paw configuration., as a function of the magnetic field.

Experimental Techniques: Thermal conductivity was measured using the 3ω technique for temperatures from 100 to 300 K on films deposited directly on silicon. A 60 nm thick $Al2O_3$ insulating layer was deposited on the capping SiN layer (20 nm), to perfectly electrically isolate the thermometers. A 5 nm thick adhesion Ti layer was deposited prior to the deposition of the Pt thermometer (95 nm thick). Four different thicknesses from 100 to 1000 nm, were measured for each sample, for disentangling the interface thermal resistance at the sample-substrate/sample-thermometer or sample-transducer interface from the intrinsic signal from the sample.[75] The analysis of the x ray diffraction pattern confirmed that the microstructure was thickness independent. Consistency of thermal measurements results indicate that there was no thickness-dependence of the thermal conductivity at all investigated temperatures between 100 nm and 1 µm, confirming previous results on pure GeTe thin films.[39,76] As mentioned in the Results section, GTC16 only had one thickness, 1µm. The thermal conductivity was measured at room temperature and the interface thermal resistance was assumed to be the same as in GTC9. As a consequence, this measurement was affected by a larger uncertainty than the one reported, and is considered as giving only an indication of the effect of an increasing carbon content. More investigations are needed for assessing the role of the carbon proportion in the samples. For the nGeTe sample, the lower annealing temperature leaves some residual stress in the thin film, which caused its delamination during the technological steps for preparing the 3ω measurements. For this reason, it was measured using the thermoreflectance technique (TR). Measurements were performed on nGeTe deposited directly on silicon. The SiN capping layer was removed and replaced by a 5 nm amorphous carbon layer and 100 nm Au film. Four different thicknesses were measured to extract the intrinsic nGeTe thermal conductivity.[77] The GeTe material annealed at 450 ° C was also measured with the TR to confirm the consistency of results between the two techniques. A value of 3.5(6) W/(m K)$^{-1}$ was obtained, against 3.8(6) W/(m K)$^{-1}$ with the 3ω technique.

Phonon dynamics at room temperature was investigated using Inelastic X ray Scattering (IXS) at the ID28 beamline of ESRF. 1 µm thick films deposited on silicon were mounted vertically and aligned in order to work close to the critical angle and reduce as much as possible the contribution form the substrate. The incoming X-ray wavelength was 0.697 Å and the energy resolution 2.8 meV. The strong small angle scattering hindered the visibility of phonons with energy smaller than 7 meV. The vibrational density of states was measured using the Inelastic X-ray Scattering technique with Nuclear resonance Analysis (IXS-NRA) at the ID18 beamline of ESRF.[54] The same films as measured by IXS were used, mounted horizontally, in a grazing incidence geometry to reduce the substrate contribution. Details on the data treatment and analysis are reported in the Supporting Information.

Electric resistivity was measured by means of the Van der Paw technique in a He-compressor between 20 and 300 K. Squared 1 cm size thin films were deposited on SOI, and gold contacts were deposited by lithography at the four corners after local removal of the SiN capping layer. The contacts with the measurement setup were thus made by wire-bonding on gold.

Theoretical Methods: The ab-initio calculation were performed using the VASP package,[78] together with PAW potentials[79,80] and the Perdew-Burke-Ernzerhof (PBE) exchange correlation functional.[81] The planewaves energy cutoff was 227 eV. The initial structure of GeTe was fully relaxed until the forces on individual atoms were less than 10−4 eV and residual stress tensor values were smaller than 0.01 kBar. To include temperature effects onto the vibrational properties, molecular dynamics simulation were performed for 15ps on a $6 \times 6 \times 6$ supercell of 432 atoms for GeTe with Gamma point sampling of the Brillouin zone using a 3fs time step and a Nosé-Hoover thermostat. The TDEP package[82] was used to compute the phonon properties at finite temperature. The TDEP fit of the second and third order forces was performed using 500 equally spaced configurations along the MD trajectory. The rhombohedral unit cell of GeTe was used for calculations. The phonon branches reported in Figure 3 have been calculated along the high symmetry directions $\Gamma - L$, $\Gamma - X$ and $\Gamma - T$, with L = [0 0.5 0], T = [0.5 0.5 0.5] and X = [0 0.5 0.5] as expressed in the relaxed reciprocal cell units. The absolute value of the directional wavevector has been calculated for plotting the dispersions together with the experimental data.

Supporting Information

Supporting Information is available from the Wiley Online Library or from the author.

Acknowledgements

The authors acknowledged fruitful discussion with A. Tanguy and K. Termentzidis, experimental help by A. Bosak, A. Chumakov and D. Bessas at ESRF. This work was financially supported by the ANR (project MAPS-ANR-20-CE05-0046 2019) and from the AURA region (Pack Ambition Recherche, project NanoCharme 2019)

Conflict of Interest

The authors declare no conflict of interest.

Author Contributions

V.M.G. and P.N. conceived and directed the project. V.M.G. conceived the phonon dynamics investigation, performed the experiments, supervised the experimental data analysis and interpretation. R. Cravero performed the thermal conductivity measurements and analysis, A. Tlili performed the inelastic x ray scattering experiments and analysis. J. Paterson and M. Tomelleri synthesized and characterized the samples in LETI clean rooms

under the supervision of P.N. J. Paterson performed also some room temperature thermal conductivity measurements. Hall measurements were performed at CEA-LETI in the framework of P. Marcello master thesis by P. Noel who is sincerely acknowledged here. R. Debord performed the low temperature Seebeck measurements. S. Pailhès participated to the discussions and interpretation. O. Bourgeois supervised the thermal measurements and participated to the discussion and interpretation. F. Hippert supervised the structural characterization and participated to discussions and interpretation. J.-Y. Raty performed the theoretical calculations and participated to discussions and interpretation. V.M.G. wrote the manuscript, the co-authors participated to the revisions.

Data Availability Statement

The data that support the findings of this study are available from the corresponding author upon reasonable request.

Keywords

interface, nanocomposite, phonons, thermal conductivity

Received: November 8, 2023
Revised: January 29, 2024
Published online: April 18, 2024

[1] G. A. Slack, *CRC Handbook of Thermoelectrics*, 1st edition, CRC Press, Boca Raton, FL **1995**, Ch. 34.
[2] K. Termentzidis, V. M. Giordano, M. Katsikini, E. Paloura, G. Pernot, D. Lacroix, T. Karakostas, J. Kioseoglou, *Nanoscale* **2018**, *10*, 21732.
[3] Y. Zhang, M. Park, S.-J. Park, *Sci. Rep.* **2019**, *9*, 2893.
[4] X. Yang, Y. Guo, X. Luo, N. Zheng, T. Ma, J. Tan, C. Li, Q. Zhang, J. Gu, *Compos. Sci. Technol.* **2018**, *164*, 59.
[5] X. Yang, L. Tang, Y. Guo, C. Liang, Q. Zhang, K. Kou, J. Gu, *Compos. - A: Appl. Sci. Manuf.* **2017**, *101*, 237.
[6] F. B. Juangsa, Y. Muroya, M. Ryu, J. Morikawa, T. Nozaki, *Appl. Phys. Lett.* **2017**, *110*, 253105.
[7] F. B. Juangsa, Y. Muroya, M. Ryu, J. Morikawa, T. Nozaki, *J. Phys. D: Appl. Phys.* **2016**, *49*, 365303.
[8] J. Moon, A. J. Minnich, *RSC Adv.* **2016**, *6*, 105154.
[9] O. Bourgeois, D. Tainoff, A. Tavakoli, Y. Liu, C. Blanc, M. Boukhari, A. Barski, E. Hadji, *C. R. Physique* **2016**, *17*, 1154.
[10] M. Verdier, K. Termentzidis, D. Lacroix, *J. Appl. Phys.* **2016**, *119*, 175104.
[11] M. Jeng, R. Yang, D. Song, G. Chen, *J. Heat Transf.* **2008**, *130*, 042410.
[12] S. V. Faleev, F. Léonard, *Phys. Rev. B* **2008**, *77*, 214304.
[13] W. Xu, Y. Liu, B. Chen, D. -B. Liu, Y. -H. Lin, A. Marcelli, *Phys. Chem. Chem. Phys.* **2013**, *15*, 17595.
[14] G. P. Srivastava, I. O. Thomas, *Nanomaterials* **2020**, *10*, 673.
[15] W. Xu, G. Zhang, *J. Phys.: Condens. Matter* **2016**, *28*, 175401.
[16] A. Tlili, V. M. Giordano, Y. M. Beltukov, P. Desmarchelier, S. Merabia, A. Tanguy, *Nanoscale* **2019**, 11, 21502.
[17] H. Luo, A. Gravouil, V. Giordano, A. Tanguy, *Nanomaterials* **2019**, *9*, 1471.
[18] H. Luo, Y. Ren, A. Gravouil, V. M. Giordano, Q. Zhou, H. Wang, A. Tanguy, *APL Mater.* **2021**, *9*, 081109.
[19] L. Yang, N. Yang, B. Li, *NanoLetters* **2014**, *14*, 1734.
[20] T. Damart, V. M. Giordano, A. Tanguy, *Phys. Rev. B* **2015**, *92*, 9.
[21] W. Schirmacher, T. Scopigno, G. Ruocco, *J. Non-Cryst. Solids* **2015**, *407*, 133.
[22] W. Schirmacher, G. Ruocco, T. Scopigno, *Phys. Rev. Lett.* **2007**, *98*, 2.
[23] Y. Beltukov, D. Parshin, V. Giordano, A. Tanguy, *Phys. Rev. E* **2018**, *98*, 023005.
[24] H. F. Hamann, M. O'Boyle, Y. C. Martin, M. Rooks, H. K. Wickramasinghe, *Nat. Mater.* **2006**, *5*, 383.
[25] P. Noé, C. Vallée, F. Hippert, F. Fillot, J. -Y. Raty, *Semicond. Sci. Technol.* **2017**, *33*, 013002.
[26] (Ed.: A. Redaelli), *Phase Change Memory: Device Physics, Reliability and Applications*, Springer International Publishing, Berlin, Heidelberg **2018**.
[27] (Ed.: A. Redaelli), *Phase Change Memory*, Springer International Publishing, Berlin, Heidelberg **2018**.
[28] J. Wei, K. Zhang, T. Wei, Y. Wang, Y. Wu, M. Xiao, *Sci. Rep.* **2017**, *7*, 1.
[29] Q. Wang, E. T. F. Rogers, B. Gholipour, C. -M. Wang, G. Yuan, J. Teng, N. I. Zheludev, *Nat. Photonics* **2015**, *10*, 60.
[30] J. Li, X. Zhang, X. Wang, Z. Bu, L. Zheng, B. Zhou, F. Xiong, Y. Chen, Y. Pei, *J. Am. Chem. Soc.* **2018**, *140*, 16190.
[31] M. Hong, J. Zou, Z. -G. Chen, *Adv. Mater.* **2019**, *31*, 1807071.
[32] M. Hong, M. Li, Y. Wang, X. -L. Shi, Z. -G. Chen, *Adv. Mater.* **2022**, *35*, 2208272.
[33] Y. Yu, M. Cagnoni, O. Cojocaru-Mirédin, M. Wuttig, *Adv. Funct. Mater.* **2020**, *30*, 1904862.
[34] Q. Hubert, C. Jahan, V. Sousa, L. Perniola, A. kusiak, J.-L. Battaglia, P. Noé, M. bernard, C. Sabbione, M. Tessaire, F. Pierre, P. Zuliani, R. annunziata, G. Pananakakis, B. de Salvo, in *Conf. on Solid State Devices and Materials (SSDM)*, **2013**, p. 550.
[35] T. -Y. Lee, K. H. P. Kim, D. -S. Suh, C. Kim, Y. -S. Kang, D. G. Cahill, D. Lee, M. -H. Lee, M. -H. Kwon, K. -B. Kim, Y. Khang, *Appl. Phys. Lett.* **2009**, *94*, 243103.
[36] G. B. Beneventi, L. Perniola, V. Sousa, E. Gourvest, S. Maitrejean, J. Bastien, A. Bastard, B. Hyot, A. Fargeix, C. Jahan, J. Nodin, A. Persico, A. Fantini, D. Blachier, A. Toffoli, S. Loubriat, A. Roule, S. Lhostis, H. Feldis, G. Reimbold, T. Billon, B. D. Salvo, L. Larcher, P. Pavan, D. Bensahel, P. Mazoyer, R. Annunziata, P. Zuliani, F. Boulanger, *Solid-State Electron.* **2011**, *65-66*, 197.
[37] D. Térébénec, N. Bernier, N. Castellani, M. Bernard, J. -B. Jager, M. Tomelleri, J. Paterson, M. -C. Cyrille, N. -P. Tran, V. M. Giordano, F. Hippert, P. Noé, *Phys. Status Solidi - Rapid Res. Lett.* **2022**, *16*, 9.
[38] R. Chahine, M. Tomelleri, J. Paterson, M. Bernard, N. Bernier, F. Pierre, D. Rouchon, A. Jannaud, C. Mocuta, V. M. Giordano, F. Hippert, P. Noé, *J. Mater. Chem. C* **2023**, *11*, 269.
[39] D. Campi, L. Paulatto, G. Fugallo, F. Mauri, M. Bernasconi, *Phys. Rev. B* **2017**, *95*, 024311.
[40] K. Ghosh, A. Kusiak, P. Noé, M. -C. Cyrille, J. -L. Battaglia, *Phys. Rev. B* **2020**, *101*, 21.
[41] A. H. Edwards, A. C. Pineda, P. A. Schultz, M. G. Martin, A. P. Thompson, H. P. Hjalmarson, *J. Phys.: Condens. Matter* **2005**, *17*, L329.
[42] G. B. Beneventi, L. Perniola, V. Sousa, E. Gourvest, S. Maitrejean, J. C. Bastien, A. Bastard, B. Hyot, A. Fargeix, C. Jahan, J. F. Nodin, A. Persico, A. Fantini, D. Blachier, A. Toffoli, S. Loubriat, A. Roule, S. Lhostis, H. Feldis, G. Reimbold, T. Billon, B. D. Salvo, L. Larcher, P. Pavan, D. Bensahel, P. Mazoyer, R. Annunziata, P. Zuliani, F. Boulanger, *Solid-State Electron.* **2011**, *65-66*, 197.
[43] A. J. Bullen, K. E. O'Hara, D. G. Cahill, O. Monteiro, A. von Keudell, *J. Appl. Phys.* **2000**, *88*, 6317.
[44] J. Li, S. J. Kim, S. Han, H. Chae, *Surf. Coat. Technol.* **2021**, *422*, 127514.
[45] A. Giri, C. J. Dionne, P. E. Hopkins, *npj Comput. Mater.* **2022**, *8*, 1.
[46] R. Jana, D. Savio, V. L. Deringer, L. Pastewka, *Modell. Simul. Mater. Sci. Eng.* **2019**, *27*, 085009.
[47] P. B. Pereira, I. Sergueev, S. Gorsse, J. Dadda, E. Müller, R. P. Hermann, *Phys. Status Solidi B* **2012**, *250*, 1300.
[48] A. Kusiak, J. -L. Battaglia, P. Noé, V. Sousa, F. Fillot, *J. Phys.: Conf. Ser.* **2016**, *745*, 032104.
[49] A. Snarskii, M. I. Zhenirovskii, I. V. Bezsudnov, *J. Thermoelectr.* **2006**, *3*, 57.

[50] H.-S. Kim, Z. M. Gibbs, Y. Tang, H. Wang, G. J. Snyder, *APL Mater.* **2015**, *3*, 041506.
[51] H. Euchner, S. Pailhès, L. T. K. Nguyen, W. Assmus, F. Ritter, A. Haghighirad, Y. Grin, S. Paschen, M. de Boissieu, *Phys. Rev. B* **2012**, *86*, 224303.
[52] P.-F. Lory, S. Pailhès, V. M. Giordano, H. Euchner, H. D. Nguyen, R. Ramlau, H. Borrmann, M. Schmidt, M. Baitinger, M. Ikeda, P. Tomes, M. Mihalkovic, C. Allio, M. R. Johnson, H. Schober, Y. Sidis, F. Bourdarot, L. P. Regnault, J. Ollivier, S. Paschen, Y. Grin, M. de Boissieu, *Nat. Commun.* **2017**, *8*, 491.
[53] V. M. Giordano, G. Monaco, *PNAS* **2010**, *107*, 21985.
[54] A. I. Chumakov, A. Q. R. Baron, R. Rüffer, H. Grünsteudel, H. F. Grünsteudel, A. Meyer, *Phys. Rev. Lett.* **1996**, *76*, 4258.
[55] T. Chatterji, S. Rols, U. D. Wdowik, *Front. Phys.* **2018**, *14*, 2.
[56] W. A. Kamitakahara, B. N. Brockhouse, *Phys. Rev. B* **1974**, *10*, 1200.
[57] W. A. Kamitakahara, D. W. Taylor, *Phys. Rev. B* **1974**, *10*, 1190.
[58] R. Gurunathan, R. Hanus, M. Dylla, A. Katre, G. J. Snyder, *Phys. Rev. Appl.* **2020**, *13*, 3.
[59] Z. Wang, J. E. Alaniz, W. Jang, J. E. Garay, C. Dames, *Nano Lett.* **2011**, *11*, 2206.
[60] A. France-Lanord, S. Merabia, T. Albaret, D. Lacroix, K. Termentzidis, *J. Phys.: Condens. Matter* **2014**, *26*, 355801.
[61] H. Gu, K. Chen, H. Wang, Z. Li, J. Wang, X. Wei, *Mater. Res. Express* **2019**, *6*, 115041.
[62] A. Minnich, G. Chen, *Appl. Phys. Lett.* **2007**, *91*, 073105.
[63] E. Pop, *Nano Res.* **2010**, *3*, 147.
[64] L. Isaeva, G. Barbalinardo, D. Donadio, S. Baroni, *Nat. Commun.* **2019**, *10*, 1.
[65] M. Simoncelli, N. Marzari, F. Mauri, *Nat. Phys.* **2019**, *15*, 809.
[66] Z. Zhang, Y. Guo, M. Bescond, J. Chen, M. Nomura, S. Volz, *APL Mater.* **2021**, *9*, 081102.
[67] Z. Zhang, Y. Guo, M. Bescond, M. Nomura, S. Volz, J. Chen, *Phys. Rev. B* **2023**, *107*, 15.
[68] R. Gu, T. Perrault, V. Juvé, G. Vaudel, M. Weis, A. Bulou, N. Chigarev, A. Levchuk, S. Raetz, V. Gusev, Z. Cheng, H. Bhaskaran, P. Ruello, *Phys. Rev. Appl.* **2021**, *16*, 1.
[69] S. Roychowdhury, M. Samanta, S. Perumal, K. Biswas, *Chem. Mater.* **2018**, *30*, 5799.
[70] J. Li, X. Zhang, Z. Chen, S. Lin, W. Li, J. Shen, I. T. Witting, A. Faghaninia, Y. Chen, A. Jain, L. Chen, G. J. Snyder, Y. Pei, *Joule* **2018**, *2*, 976.
[71] Y. Chen, C. M. Jaworski, Y. B. Gao, H. Wang, T. J. Zhu, G. J. Snyder, J. P. Heremans, X. B. Zhao, *New J. Phys.* **2014**, *16*, 013057.
[72] M. Samanta, S. Roychowdhury, J. Ghatak, S. Perumal, K. Biswas, *Chem. - Eur. J.* **2017**, *23*, 7438.
[73] Y. Gelbstein, J. Davidow, *Phys. Chem. Chem. Phys.* **2014**, *16*, 20120.
[74] G. E. Ghezzi, J. Y. Raty, S. Maitrejean, A. Roule, E. Elkaim, F. Hippert, *Appl. Phys. Lett.* **2011**, *99*, 15.
[75] J. Paterson, D. Singhal, D. Tainoff, J. Richard, O. Bourgeois, *J. Appl. Phys.* **2020**, *127*, 24.
[76] R. J. Warzoha, B. F. Donovan, N. T. Vu, J. G. Champlain, S. Mack, L. B. Ruppalt, *Appl. Phys. Lett.* **2019**, *115*, 023104.
[77] M. Hadi, S. Pailhès, R. Debord, A. Benamrouche, E. Drouard, T. Gehin, C. Botella, J. -L. Leclercq, P. Noe, F. Fillot, V. Giordano, *Materialia* **2022**, *26*, 101574.
[78] G. Kresse, J. Hafner, *Phys. Rev. B* **1994**, *49*, 14251.
[79] P. E. Blöchl, *Phys. Rev. B* **1994**, *50*, 17953.
[80] G. Kresse, D. Joubert, *Phys. Rev. B* **1999**, *59*, 1758.
[81] J. P. Perdew, K. Burke, M. Ernzerhof, *Phys. Rev. Lett.* **1997**, *78*, 1396.
[82] O. Hellman, P. Steneteg, I. A. Abrikosov, S. I. Simak, *Phys. Rev. B* **2013**, *87*, 10.